

Quasi-3D Geoelectrical Imaging as A New Application for Landslide Investigations: A Tunnel Case Induced by Blasting Activity

Rudi Cahyadi¹, Widodo Widodo²

¹Department of Physics, Universitas Andalas, Padang, 25163, Indonesia

²Geophysical Engineering, Institute of Technology Bandung, Bandung 40132, Indonesia

Article Info

Article History:

Received July 16, 2024

Revised August 18, 2024

Accepted August 24, 2024

Published August 30, 2024

Keywords:

geoelectrical

high-speed railway tunnel

landslide

quasi-3D

resistivity

Corresponding Author:

Rudi Cahyadi

Email:

rudi.cahyadi@sci.unand.ac.id

ABSTRACT

Landslides are a significant hazard in mountainous regions, especially when influenced by construction activities such as tunnel excavation. In this paper, we aim to conduct a slope stability analysis as a result of tunnel blasts using quasi-3D subsurface models based on resistivity values. The study site is a construction area for the Jakarta-Bandung High-Speed Train tunnel, located in a mountainous region undergoing drill-and-blast excavation. This excavation method makes the area susceptible to landslides, which pose a threat to settlements in the Padalarang subdistrict, West Bandung Regency, Indonesia. Data was collected along four lines in 2D, and the dipole-dipole array was used to enhance resolution. Data modeling was carried out using ResIPy v3.2.3 software to create 2D and quasi-3D subsurface models based on resistivity values. The study findings indicate that the study area exhibits three resistivity ranges: low resistivity (0-30 Ωm), medium resistivity (31-49 Ωm), and high resistivity (>50 Ωm). Utilizing quasi-3D imaging, we were able to identify the dimensions and presence of slip surfaces, which can be categorized as shallow (1.5-5 m) and deep (5-20 m) criteria. This study successfully applied the quasi-3D geoelectrical approach in a susceptible environment to detect potential landslide zones.

Copyright © 2024 Author(s)

1. INTRODUCTION

One ongoing infrastructure project is the construction of a tunnel for the Jakarta-Bandung High-Speed Train railway. This project is being carried out by PT. Kereta Cepat Indonesia-China (KCIC) in collaboration with PT. China Railway Group Limited (CREC). The main tunnel, designated as Tunnel 11, will be excavated through Mount Bohong (Figure 1(a)) using a drill-and-blast technique. Tunnel 11 is located in the Padalarang sub-district of the West Bandung Regency in West Java Province, Indonesia. Evaluating the slope stability of Mount Bohong is crucial to assess its ability to withstand vibrations from the blasting activity both during and after construction.

The primary aim of this research is to conduct a comprehensive slope stability analysis to ensure the structural safety of Tunnel 11. This involves utilizing subsurface soil investigation methods, including advanced geophysical techniques. The study is motivated by the need to address the potential

risks posed by the excavation activities and to contribute valuable insights into effective risk management strategies for similar large-scale infrastructure projects.

Geophysical methods have proven to be indispensable tools in subsurface investigations, offering insights into subsurface modeling, geological structure mitigation, hazard assessment, near-surface feature mapping, hydrological studies, and engineering applications (Widodo et al., 2016; 2018; Binley et al., 2015; Devi et al., 2020). Among these methods, the electrical resistivity or geoelectrical method has emerged as a powerful technique. It is utilized in various formats, including 1D, 2D, Quasi-3D, and 3D configurations, and has garnered significant attention for solving engineering problems (Giocoli et al., 2019; Lech et al., 2020; Pazzi et al., 2018; Zakaria et al., 2021). The evolution of instrumentation, data inversion, and advancements in computer technology have significantly enhanced the efficacy and popularity of geoelectrical methods in subsurface investigations (Loke et al., 2013). These methods are now firmly established for studying landslides on unstable slopes (Jongmans & Garambois, 2007).

The quasi-3D geoelectrical method, in particular, has emerged as an invaluable tool in modern geophysical investigations. This research highlights the method's ability to provide a high-resolution view of resistivity distribution below the Earth's surface, thereby allowing for the detection of resistivity variations across different depths and spatial areas. Unlike conventional 2D geoelectrical methods, quasi-3D offers enhanced resolution in localized regions, facilitating a more precise assessment of high-risk areas. The ability to visualize data in three-dimensional models significantly improves the interpretation of subsurface structures and geological features, which is essential for understanding slope stability and developing effective risk management strategies. This study contributes to the growing body of knowledge by applying the quasi-3D geoelectrical method to a real-world scenario, demonstrating its effectiveness in addressing contemporary challenges in geohazards and environmental assessments.

Previous investigations at this research site have included groundwater condition studies by Phanjaya et al., (2022) and initial slope stability analyses by Widodo et al., (2023), which involved PPA and PPV methods for assessing soil conditions. By building on this foundation, the current research aims to offer a more detailed and accurate assessment of slope stability, providing critical insights for both current and future infrastructure projects.

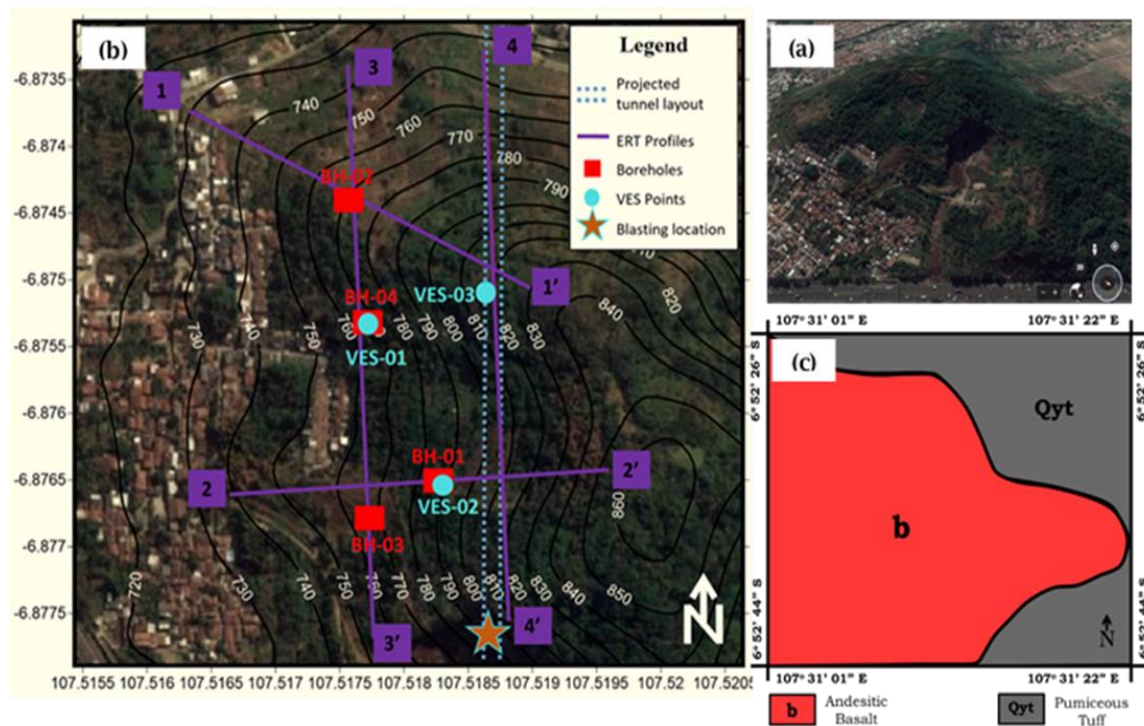


Figure 1 (a) Mount Bohong, (b) Geoelectrical survey lines, and (c) Geological information.

2. METHOD

2.1 Data Collection

The geoelectrical survey was conducted using an Ares II multi-channel resistivity meter. The measurements were taken along four lines with an overlapping dipole-dipole configuration. The specific array geometric parameters can be found in Table 1. The variation in electrode spacing was due to the difference in line length, which was 350 m for Lines 1 and 2 and 470 m for Lines 3 and 4. As a result, for quasi-3D processing, the lines were divided into two parts: Part 1 for Lines 1 and 2, and Part 2 for Lines 3 and 4.

In geoelectrical survey (Figure 1(b)), the entire set of electrodes shifts laterally by one electrode separation after each measurement. This comprehensive approach ensures thorough data collection. For our survey, we adopted a dipole-dipole configuration, optimizing current and potential electrode placement for accurate readings. The distance between the nearest current and potential electrode is n times the basic distance a , as illustrated in Figure 2(b), showcasing our meticulous attention to detail. The apparent resistivity value is accurately determined by plotting it at the point where two converging lines intersect at a 45° angle, drawn from the centers of the current and potential electrodes (Reynolds, 2011; Binley & Slater, 2020). Apart from that, we also require information about the geology of the research area (Figure 1(c)) to conduct a more comprehensive analysis.

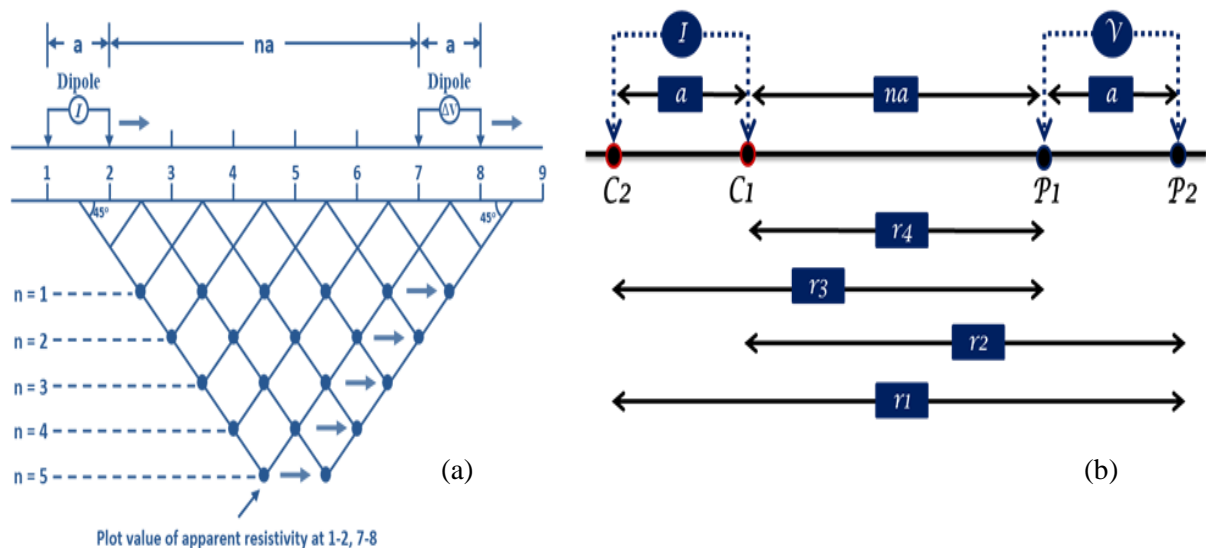


Figure 2 Dipole–dipole array: (a) method of plotting apparent resistivity data in pseudo-section. (b) electrodes arrangement, n represents the relative spacing between the current (C) and potential (P) dipoles.

This research provides four pieces of supporting data for drilling operations, with each borehole reaching a depth of 20 meters. The locations of the boreholes are detailed in Figure 1(b). Samples obtained from the boring process were carefully selected for laboratory analysis. The results reveal the presence of three distinct lithological units in the area: silty clay, gravelly clay, and andesite breccia, as seen in Figure 3.

Table 1 Geometric parameters of dipole-dipole array

Geometric Parameters	Profile Line			
	1	2	3	4
Length of line (m)	322	322	430	430
Number of electrodes	48	48	48	48
Electrodes spacing (m)	7.5	7.5	10	10
Max n level	5	5	5	5

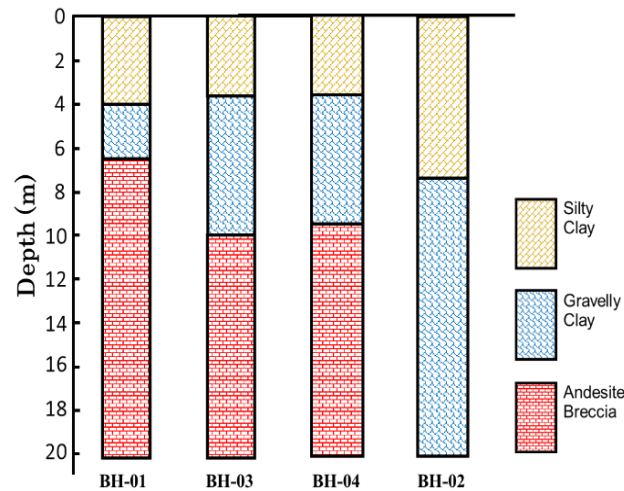


Figure 3 Lithological information according to sample based on borehole data.

2.2 Data Processing

In our research, we utilized ResIPy software, a Python-based program capable of conducting inversion in both 2D and 3D within a single application package. The basis for the development of ResIPy is Gaussian Newton inversion. The 3D inversion iteration process in ResIPy is governed by the following equation (Binley & Slater, 2020):

$$(J^T W_d^T W_d J + \alpha R) \Delta m = J^T W_d^T (d - f(m_i)) - \alpha R m \tag{1}$$

$$m_{i+1} = m_i + \Delta m \tag{2}$$

where J is the Jacobian, such that $J_{ij} = \partial d / \partial m$, d is the data vector, m_i is the parameter vector at iteration i , W_d is the data weight matrix, assumed to be diagonal, with diagonal values $W_{i,i} = 1/\epsilon_i$, where ϵ_i is the standard deviation of measurement i , α is the regularisation (or smoothing) parameter, R is the roughness matrix, which describes the connectivity of parameter blocks, Δm is update in parameter values at each iteration, and $f(m)$ is the forward model for parameters m .

Equations (1) and (2) are iterated until sufficient convergence conditions are met, as determined by the data misfit reaching the required tolerance. If the data misfit is expressed as a Root Mean Square (RMS) error, the formulation used is as follows:

$$RMS = \sqrt{\frac{1}{N} \left(\frac{d - f_i(m)}{\hat{\sigma}} \right)^2} \tag{3}$$

where N in the Equation (3) is the number of measurements, then the target tolerance should be 1, following a chisquared distribution.

3. RESULTS AND DISCUSSION

3.1 2D Inversion Results

Based on the 2D inversion results, as seen in Figure 4 (right), we observed three ranges of resistivity values at the research location: low, medium, and high resistivity. The low resistivity is indicated in blue and ranges from 0 to 30 Ωm , the medium resistivity is indicated in green-yellow and ranges from 31 to 49 Ωm , and the high resistivity is indicated in red starting from 50 Ωm . The parameters of the 2D inversion results can be seen in Table 2. The data obtained from the boreholes confirms that the upper layer comprises silty clay, the middle layer consists of gravelly clay, and the substratum layer is composed of andesite breccia, as evidenced by BH-01 and BH-04. Notably, all inversion results

produced a low RMS value of less than 2%, indicating a robust agreement between the calculated and measured data.

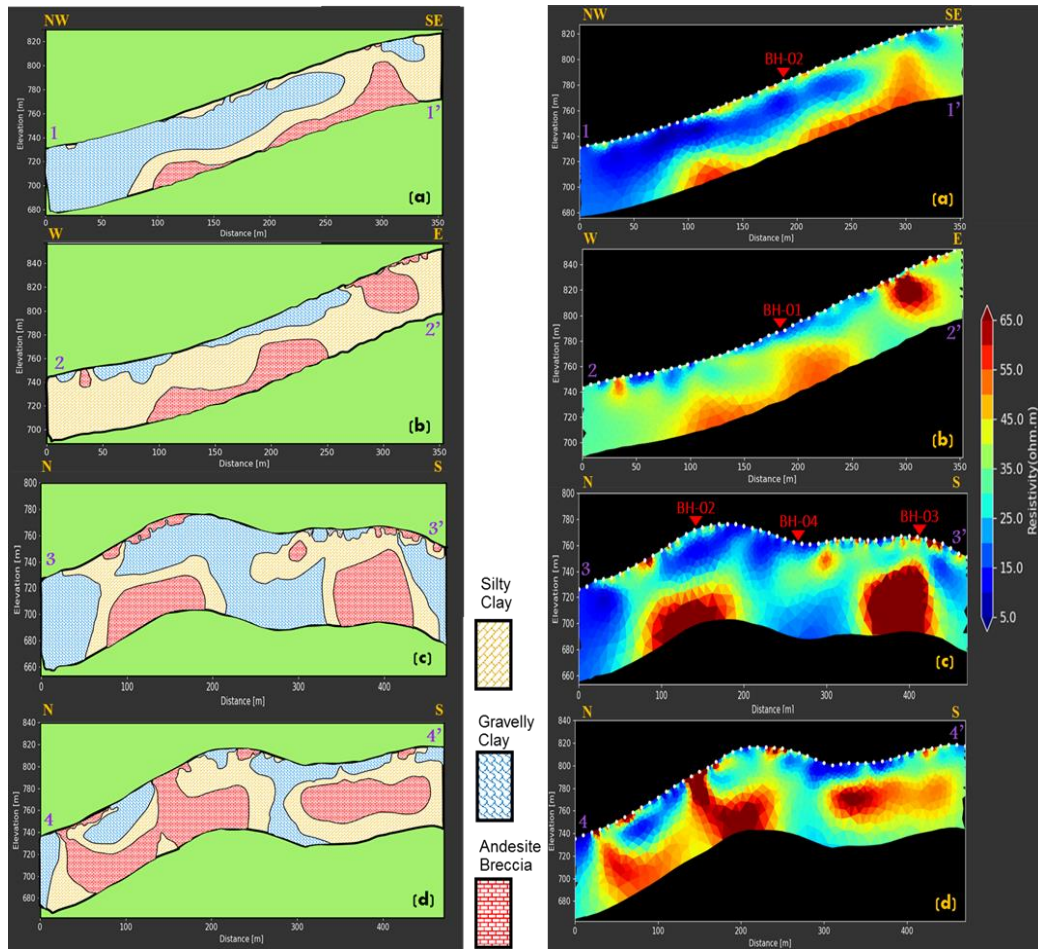


Figure 4 Image of 2D inversion (right) and correlation to boreholes data (left) results.

The survey indicates the following resistivity values along two perpendicular lines on a mount slope. Line 1, see Figure 4(a), extends in a northwest-southeast direction, with low resistivity values (0 – 30 Ωm) observed from the first electrode to a distance of 270 m at depths of 0 – 30 m. At a distance of 100 m, these values are found at depths of 7.5 – 25 m, extending to 100 – 270 m. Medium resistivity values of 31 – 49 Ωm are seen at depths of 0 – 7.5 m and 30 – 45 m at distances of 115 – 250 m, and distances of 250 – 350 m, these values are found at depths varying from 0 – 40 m. High resistivity values (> 50 Ωm) are found starting at a depth of 40 m at a distance of 75 – 145 m and are visible at a distance of 90 – 335 m at a depth ranging from 20 – 50 m. This inversion results clearly demonstrate high resistivity contrast at shallow and intermediate depths, aligning perfectly with the BH-02 stratigraphical data.

Table 2 Parameters of 2D inversion results

2D Inversion Parameters	Profiles			
	L1	L2	L3	L4
Iteration	1	2	2	2
Roughness	32.9	24.4	66.4	97.3
Final RMS Misfit	1.25	1.00	1.00	1.26
Total Memory Required (Gb)	0.090	0.085	0.086	0.087
Number of Measurements Read	850	852	848	849

Line 2, see Figure 4(b), runs in a west-east direction, with low resistivity values of 0 – 30 Ωm observed on the surface. This range is visible at distances of 5 – 20 m with a depth of 0 – 7 m, at distances of 45 – 110 m with a depth range of 0 – 15 m, and at distances of 130 – 275 m with depths varying from 0 – 20 m. Medium resistivity values of 31 – 49 Ωm are observed at distances of 0 – 285 m with depths ranging from 0 – 50 m, and at distances of 310 – 350 m they are found at depths between 7 – 50 m. High resistivity values of > 50 Ωm are initiated from a depth of 0 – 20 m at distances of 0 – 40 m, from a depth of 10 – 35 m at distances of 95 – 250 m, and from a depth of 0 – 40 m at distances of 265 – 335 m. Furthermore, the resistivity contrast indicated in this inversion model is consistent with the findings from the BH-01 borehole in this profile.

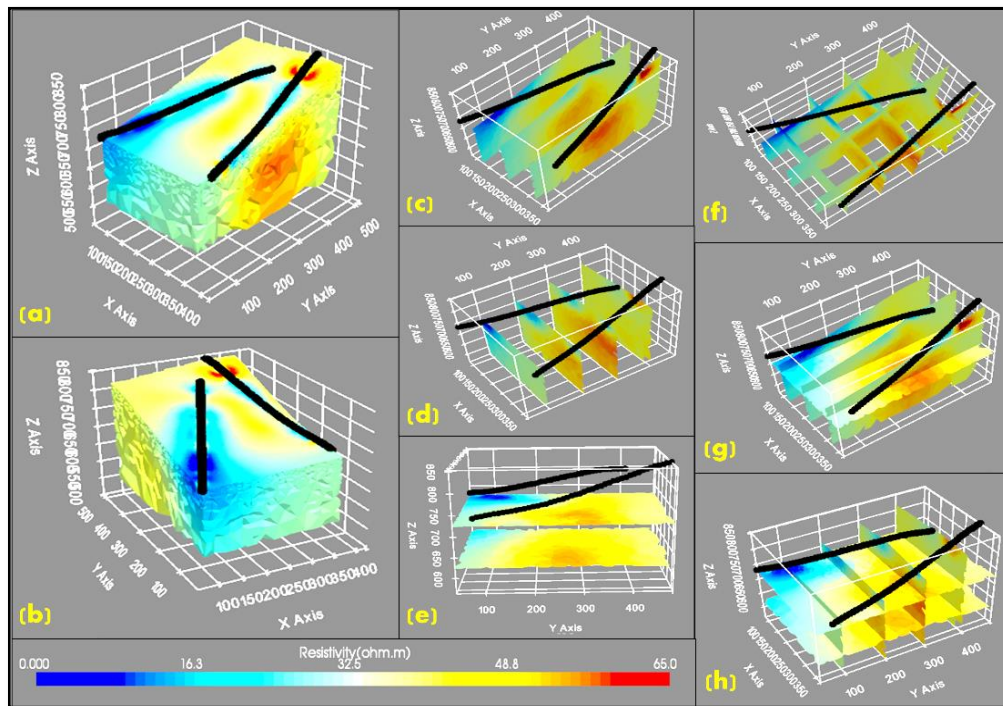


Figure 5 (a) and (b) inversion results of quasi-3D of Lines 1 and 2, (c) slices in the X direction, (d) slices in the Y direction, (e) slices in the Z direction, (f) slices in the X and Y directions, (g) slices in the X and Z directions, and (h) slices in the Y and Z directions. According to Figure (a), Line 1 is located on the left-hand side, along the Y-axis direction.

Lines 3 and 4 are cross-perpendicular to the slope, in a north-south direction. The first electrode is in the north. In Line 3, low resistivity values are observed between 100 – 330 m distances, with depths ranging from 0 – 50 m. High resistivity values are visible at 80 – 180 m distance starting at a depth of 30 m and 350 – 420 m distance starting at a depth of 20 m. High resistivity is also noticeable on the surface at distances of 40 – 90 m and 390 – 440 m with shallow depths of 0 – 10 m, see Figure 4(c). The inversion result in Line 3 does not align well with the BH-04 and BH-03 boreholes, but the BH-02 borehole fits the resistivity model in the Line 1 profile. The silty clay formation in this profile exhibits high resistivity in the southern part, low resistivity in the central zone, and moderate resistivity in the northern area. The varying resistivity of the silty clay can be explained similarly to the silty clay in the Line 1 and 2 profiles, respectively.

In Line 4, which is directly above tunnel 11, low resistivity values of 0 – 30 Ωm are visible at a distance of 50 – 120 m with a depth of 0 – 30 m, at a distance of 175 – 230 m with a depth of 0 – 25 m, and a distance of 250 – 410 m with a depth of 0 – 50 m. High resistivity values are found at a distance of 30 – 240 m with depths varying from 0 – 50 m, and at a distance of 300 – 450 m at a depth of 20 – 50 m, see Figure 4(d). Unfortunately, there were no boreholes available in this area for interpretation. As a result, we depended on the information from Line 3 for our analysis. The resistivity image displays

results that are quite similar to the wide resistivity variation seen in the Line 3 profile. The medium resistivity values are between the two ranges of resistivity values mentioned above.

Table 3 Parameters of quasi-3D inversion results

Quasi-3D Inversion Parameters	Profiles	
	Lines 1 and 2	Lines 3 and 4
Iteration	2	2
Roughness	54.3	220.9
Final RMS Misfit	1.02	1.01
Total Memory Required (Gb)	2.722	0.743
Number of Measurements Read	1702	1697

3.2 Quasi-3D Inversion Results

The results of the quasi-3D inversion generally show resistivity cross-sections that are very similar to the 2D inversion results. The presence of low, medium, and high resistivity is appropriate. Due to this reason, the range of resistivity values utilized in the quasi-3D inversion remain consistent with those employed in the previous iteration. The quasi-3D inversion results for Lines 1 and 2 show similar findings to the 2D inversion results. They indicate the presence of high resistivity beneath line 2 (Figure 5). This pattern is also observed in Lines 3 and 4 (Figure 6), which show high resistivity at a distance of 350 to 450 meters. The distribution of low resistivity in Lines 1 and 2 is quite clear, and can be utilized for further interpretation. The parameters of the quasi-3D inversion results can be seen in Table 3. In this table, the number of datum points to be executed (last row) is the sum of the datum points of two parallel lines. It can be seen that the more data points, the greater the memory required.

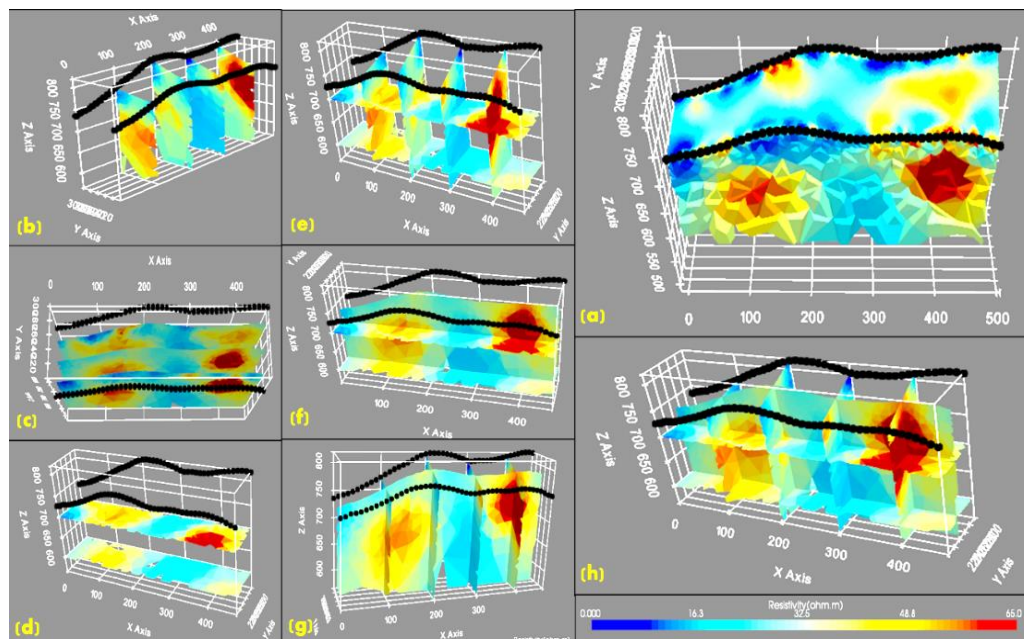


Figure 6 (a) Quasi-3D inversion results of Lines 3 and 4, (b) slices in the X direction, (c) slices in the Y direction, (d) slices in the Z direction, (e) slices in the X and Z directions, (f) slices in the Y and Z directions, (g) slices in the X and Y directions, and (h) slices in the X, Y, and Z directions. According to Figure (a), Line 3 is positioned in front, along the X-axis direction.

3.3 Landslide Analysis

To achieve a thorough understanding of potential landslide zones, integrating insights from both quasi-3D and 2D inversion analyses is crucial. Both methods highlight the significance of the slip plane in identifying these zones, but they do so from different perspectives. The quasi-3D analysis provides a

broader view of the slip plane's alignment and its spatial relationship with the slope, offering a contextual understanding of its position. In contrast, the 2D inversion delivers precise, depth-specific information that reveals critical resistivity contrasts essential for determining the exact depths of potential landslides. While the quasi-3D approach effectively maps the general orientation of the slip plane, it relies on complementary 2D inversion data to accurately delineate potential landslide areas. Conversely, the 2D inversion pinpoints resistivity changes that are crucial for understanding the depth and extent of landslide risks.

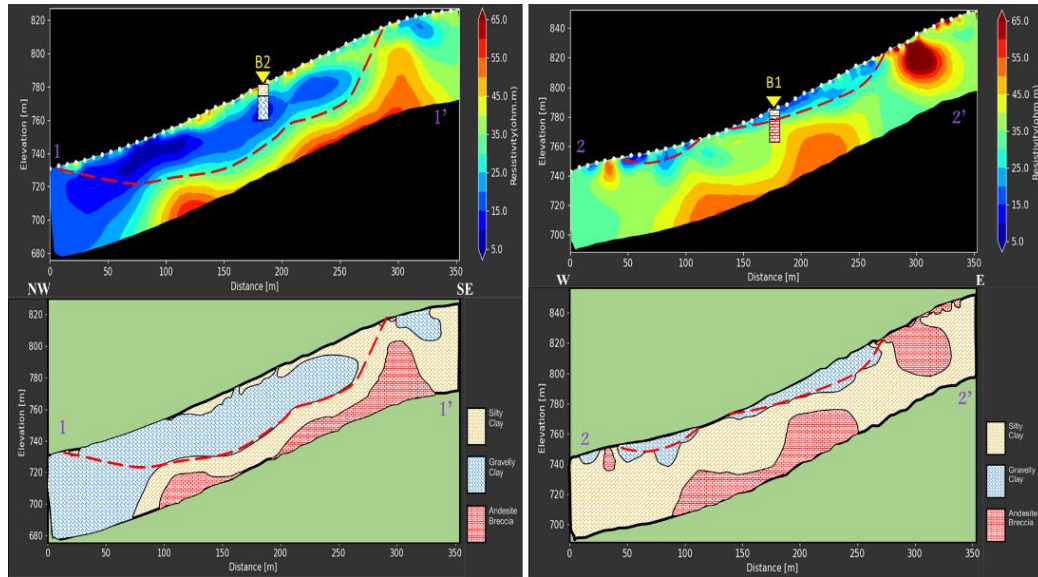


Figure 7 Suspected areas with potential for landslides on Lines 1 and 2.

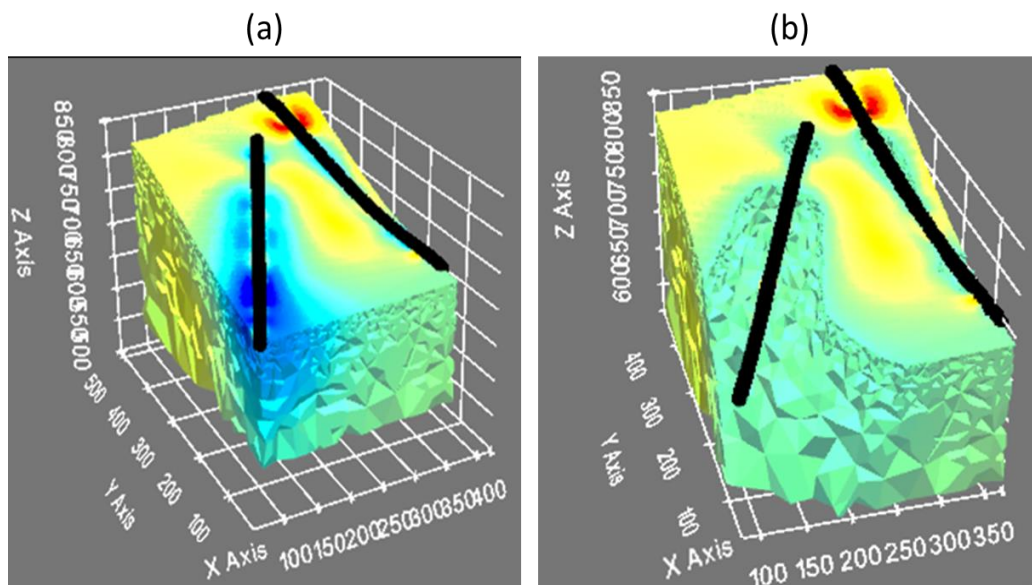


Figure 8 (a) Estimated dimensions of the slip plane area (low resistivity) in quasi-3D inversion of Lines 1 and 2 and (b) after excluding low resistivity values.

The 2D inversion analysis reveals potential landslide areas and slip planes within the mount penetrated by tunnel 11, with significant observations along Lines 1 and 2. Line 1 demonstrates a clear contrast between high and low resistivity values, suggesting the presence of slip planes. This contrast indicates a layer of softer material overlying a more resistant substrate, particularly evident from the

first electrode to a distance of 250 m. Line 2 identifies two additional suspected landslide zones: one between 45 – 110 m and another between 150 – 265 m, with soft material extending up to 40 m in depth as shown in Figure 7.

The quasi-3D inversion further refines these findings by situating the slip plane along Lines 1 and 2, perpendicular to the slope. To accurately determine potential landslide areas, it is necessary to distinguish low resistivity zones from medium and high resistivity regions. The 2D inversion highlights that the low resistivity zone, if excluded from the quasi-3D cross-section, could indicate a potential landslide area, as illustrated in Figure 8. The quasi-3D model extends the 2D results into a 3D context, enhancing the spatial resolution. Following the removal of low resistivity values, Figure 8 reveals a prominent and relatively deep depression along Line 1, contrasting with a smaller, shallower depression along Line 2 where low resistivity values are primarily surface-bound.

This integrated approach, combining 2D and quasi-3D analyses, provides a more detailed and nuanced assessment of potential landslide areas than either method alone. By leveraging the strengths of both techniques, this research offers a more comprehensive evaluation of the slip plane's impact, thus enhancing confidence in the findings and supporting more informed decision-making in landslide risk assessment.

This research contributes novel insights by leveraging both 2D and quasi-3D geoelectrical methods to provide a comprehensive evaluation of landslide risks. The integration of these methods offers a detailed and robust assessment of the slip plane's impact, enhancing the accuracy and reliability of landslide risk evaluations. This approach not only improves the interpretative depth but also supports more informed decision-making in infrastructure projects, particularly in complex geological settings.

Although quasi-3D electrical resistivity tomography and similar software were previously utilized by Cheng et al., (2019) to investigate karst structures, their approach focused on assembling results from a series of 2D slices arranged like a network, which is akin to a sliced model of volume. In contrast, our study presents results in a complete volumetric format derived from two 2D profiles, with low resistivity components removed to project potential landslide areas. The strong support from the 2D results enabled the creation of a high-quality quasi-3D model. We emphasize that without relevant and supportive 2D data, producing a comprehensive quasi-3D volumetric model, as demonstrated in our study, would be challenging.

In summary, our approach demonstrates the effectiveness of integrating 2D and quasi-3D geoelectrical methods in assessing landslide risks, offering a more detailed and accurate evaluation of potential landslide zones. This method enhances both the precision of risk assessment and the robustness of geological modeling, providing valuable insights for future infrastructure planning and risk management in complex terrains.

4. CONCLUSION

Based on the results of 2D and quasi-3D inversion, it has been determined that the research area exhibits three distinct resistivity ranges: low resistivity of 0 – 30 Ωm , medium resistivity of 31 – 49 Ωm , and high resistivity greater than 50 Ωm . Additionally, it is known that the western portion of the research area has dimensions of the slip area, which varies from shallow depth criteria (1.5 - 5 m) to deeper depths (5 - 20 m). The results of quasi-3D inversion have indicated that ResIPy is capable of effectively and efficiently producing inversions of 2D pseudo resistivity data, resulting in equivalent shapes to the 3D model. This quasi-3D method also proves to be valuable in describing the potential of landslides by revealing detailed subsurface features and variations. Thus, this study successfully applied the quasi-3D geoelectrical approach in a susceptible environment to detect potential landslide zones.

ACKNOWLEDGEMENT

This research received financial support from research grants awarded to Widodo Widodo by LPPM (Institute for Research and Community Services) under the P3MI-ITB scheme for fiscal year 2020, from the Bandung Institute of Technology, and from RISTEK DIKTI (Ministry of Research, Technology, and Higher Education of the Republic of Indonesia). The author acknowledges the

Indonesia Endowment Fund for Education (LPDP) from the Ministry of Finance of the Republic of Indonesia for granting a scholarship and supporting this research. The author expresses gratitude to the editorial team of Jurnal Ilmu Fisika (JIF) and the anonymous reviewers.

REFERENCES

- Binley, A., Hubbard, S. S., Huisman, J. A., Revil, A., Robinson, D. A., Singha, K., & Slater, L. D. (2015). The emergence of hydrogeophysics for improved understanding of subsurface processes over multiple scales. *Water Resources Research*, 51(6), 3837–3866. <https://doi.org/10.1002/2015WR017016>.
- Binley, A., & Slater, L. (2020). *Resistivity and induced polarization: Theory and applications to the near-surface earth*. Cambridge University Press. <https://doi.org/10.1017/9781108685955>.
- Cheng, Q., Chen, X., Tao, M., & Binley, A. (2019). Characterization of karst structures using quasi-3D electrical resistivity tomography. *Environmental Earth Sciences*, 78, 1–12. <https://doi.org/10.1007/s12665-019-8284-2>.
- Devi, A., Israil, M., Singh, A., Gupta, P. K., Yogeshwar, P., & Tezkan, B. (2020). Imaging of groundwater contamination using 3D joint inversion of electrical resistivity tomography and radio magnetotelluric data: A case study from Northern India. *Near Surface Geophysics*, 18(3), 261–274. <https://doi.org/10.1002/nsg.12092>.
- Giocoli, A., Hailemikaël, S., Bellanova, J., Calamita, G., Perrone, A., & Piscitelli, S. (2019). Site and building characterization of the Orvieto Cathedral (Umbria, Central Italy) by electrical resistivity tomography and single-station ambient vibration measurements. *Engineering Geology*, 260, 105195. <https://doi.org/10.1016/j.enggeo.2019.105195>.
- Jongmans, D., & Garambois, S. (2007). Geophysical investigation of landslides: a review. *Bulletin de La Société Géologique de France*, 178(2), 101–112. <https://doi.org/10.2113/gssgfbull.178.2.101>.
- Lech, M., Skutnik, Z., Bajda, M., & Markowska-Lech, K. (2020). Applications of electrical resistivity surveys in solving selected geotechnical and environmental problems. *Applied Sciences*, 10(7), 2263. <https://doi.org/10.3390/app10072263>.
- Loke, M. H., Chambers, J. E., Rucker, D. F., Kuras, O., & Wilkinson, P. B. (2013). Recent developments in the direct-current geoelectrical imaging method. *Journal of Applied Geophysics*, 95, 135–156. <https://doi.org/10.1016/j.jappgeo.2013.02.017>.
- Pazzi, V., Di Filippo, M., Di Nezza, M., Carlà, T., Bardi, F., Marini, F., Fontanelli, K., Intrieri, E., & Fanti, R. (2018). Integrated geophysical survey in a sinkhole-prone area: Microgravity, electrical resistivity tomographies, and seismic noise measurements to delimit its extension. *Engineering Geology*, 243, 282–293. <https://doi.org/10.1016/j.enggeo.2018.07.016>.
- Phanjaya, H., Parnadi, W. W., & Santoso, D. (2022). Electrical resistivity survey for groundwater investigation in Padalarang, West Java. *IOP Conference Series: Earth and Environmental Science*, 1031(1), 012006. <https://doi.org/10.1088/1755-1315/1031/1/012006>.
- Reynolds, J. M. (2011). *An introduction to applied and environmental geophysics*. John Wiley & Sons.
- Widodo, Gurk, M., & Tezkan, B. (2016). Multi-dimensional interpretation of radiomagnetotelluric and transient electromagnetic data to study active faults in the Mygdonian Basin, Northern Greece. *Journal of Environmental and Engineering Geophysics*, 21(3), 121–133. <https://doi.org/10.2113/JEEG21.3.121>.
- Widodo, Phanjaya, H., Prassettyo, S. H., Simangunsong, G. M., Rai, M. A., & Wattimena, R. K. (2023). Dynamic Slope Stability Subject to Blasting Vibrations: a Case Study of the Jakarta-Bandung High-Speed Railway Tunnel. *Transportation Infrastructure Geotechnology*, 10(5), 774–794. <https://doi.org/10.1007/s40515-022-00242-6>.
- Widodo, W., Azimmah, A., & Santoso, D. (2018). Exploring the Japan Cave in Taman Hutan Raya Djuanda, Bandung using GPR. *Journal of Environmental and Engineering Geophysics*, 23(3), 377–381. <https://doi.org/10.2113/JEEG23.3.377>.
- Zakaria, M. T., Mohd Muztaza, N., Zabidi, H., Salleh, A. N., Mahmud, N., Samsudin, N., Rosli, F. N., Olugbenga, A. T., & Jia, T. Y. (2021). 2-D cross-plot model analysis using integrated geophysical methods for landslides assessment. *Applied Sciences*, 11(2), 747. <https://doi.org/10.3390/app11020747>.